Open access • Posted Content • DOI:10.1101/2020.07.16.206953

Drone phenotyping and machine learning enable discovery of loci regulating daily floral opening in lettuce — Source link

Rongkui Han, Andy J. Y. Wong, Zhehan Tang, Maria Jose Truco ...+4 more authors

Institutions: University of California, Davis, University of California

Published on: 16 Jul 2020 - bioRxiv (Cold Spring Harbor Laboratory)

Topics: Population

Drone phenotyping and machine learning enable discovery of loci regulating daily floral opening in lettuce

Short title: Genetics of floral opening time with drone data

Rongkui Han[1], Andy J.Y. Wong[2], Zhehan Tang[2], Maria J. Truco[1], Dean O. Lavelle[1], Alexander Kozik[1], Yufang Jin[2], Richard W. Michelmore[1*]

Affiliations

[1]: The Genome and Biomedical Sciences Facility, University of California, Davis

[2]: Department of Land, Air and Water Resources, University of California, Davis

*: Author for contact

Author Contributions

RM, MJT, DL, and RH conceived the experiment. RH designed and conducted the field experiment, performed the data analysis including the machine learning, Bayesian inference, and genetic mapping, and drafted the paper. AW, ZT, and YJ performed the drone phenotyping and assisted in the image analysis. MJT and DL developed the mapping population and genotyped by sequencing. AK made the video of asynchronous flower opening. All authors contributed to writing the paper.

One sentence summary

Machine learning and Bayesian analyses of drone-mediated remote phenotyping data revealed two genetic loci regulating differential daily flowering time in lettuce (*Lactuca spp.*).

Abstract

Flower opening and closure are traits of reproductive importance in all angiosperms because they determine the success of self- and cross-pollination. The temporal nature of this phenotype rendered it a difficult target for genetic studies. Cultivated and wild lettuce, *Lactuca spp.*, have composite inflorescences comprised of multiple florets that open only once. Different accessions were observed to flower at different times of day. An F_6 recombinant inbred line population (RIL) had been derived from accessions of *L. serriola* x *L. sativa* that originated from different environments and differed markedly for daily floral opening time. This population was used to map the genetic determinants of this trait; the floral opening time of 236 RILs was scored over a seven-hour period using time-course image series obtained by drone-based remote phenotyping on two occasions, one week apart. Floral pixels were identified from the images using a support vector machine (SVM) machine learning algorithm with an accuracy above 99%. A Bayesian inference method was developed to extract the peak floral opening time for individual genotypes from the time-stamped image data. Two independent QTLs, *qDFO2.1* (*Daily Floral Opening* 2.1) and *qDFO*8.1, were discovered. Together, they explained more than 30% of the phenotypic variation in floral opening time. Candidate genes with non-synonymous polymorphisms in coding sequences were identified within the QTLs. This study demonstrates the power of combining remote imaging, machine learning, Bayesian statistics, and genome-wide marker data for studying the genetics of recalcitrant phenotypes such as floral opening time.

Keywords: flowering, flower opening, genetic mapping, QTL mapping, lettuce, drone, unmanned aerial vehicle (UAV), high-throughput phenotyping, remote sensing phenotyping, image analysis, machine learning, support vector machine (SVM), Bayesian inference

47

48 **Introduction**

49 Floral opening is a complex and dynamic process marked by rapid, drastic changes in the
50 morphology of the reproductive organs of angiosperms. The time of floral opening marks the onset
51 of the period during which cross pollination becomes possible, making this physiological process
52 a critical phase in plant sexual reproduction. From an ecological perspective, different floral
53 opening times within the day can play an important role in population divergence by contributing
54 to temporal reproductive isolation (Matsumoto et al., 2013). Synchronizing floral opening time
55 with peak activity of effective pollinators may help improve outcrossing and reproductive success
56 (Sakamoto et al., 2012).

57

58 Across different flowering species, successful floral opening is accomplished through a diverse set
59 of events—petals may unfold, spiral outward, or spring open, depending on their particular
60 anatomies, and the opening process may or may not be reversible. What usually underlies these
61 impressive local movements is a high rate of cell expansion and/or abscission driven by changes
62 in osmotic pressures. The timing of this process is regulated by external and internal factors.
63 Environmental cues, such as humidity, temperature, and light, the internal circadian rhythm of the
64 plant, and hormone signaling all modulate floral opening (van Doorn and van Meeteren, 2003; van
65 Doorn and Kamdee, 2014). Different species show various levels of responsiveness to these
66 internal and external cues. In extreme cases, the effect of the same signal can be completely
67 opposite in different species. For instance, ethylene treatment is known to accelerate floral opening
68 in some rose (*Rosa spp.*) cultivars, while inhibiting floral opening in others (Reid *et al.* 1989).

69

The molecular control of floral opening is incompletely understood. Past endeavors to probe regulation of floral opening have mainly taken four approaches: gene transcription, cellular signaling, mutant analysis, and forward genetics. Transcription-level events corresponding to the physiological process of floral opening have been detected in multiple studies. High accumulation of volatile-emission-related R2R3-MYB transcription factor EOBII was found in hybrid peas (*Pisum x hybrida* "Mitchell Diploid") and *Nicotiana attenuata* prior to floral opening. RNAi knockdown of EOBII resulted in failure to enter anthesis and premature senescence (Colquhoun et al., 2011). Over-expression of fructan 1-exohydrolase was associated with flower opening in *Campanula rapunculoides*, presumably contributing to decreasing osmotic pressure in expanding petals by breaking down polysaccharide fructan (Vergauwen et al., 2000; Le Roy et al., 2007). Similarly, transcriptional upregulation of cell-wall-loosening expansin was associated with floral opening in carnation (*Dianthus caryophyllus*; Harada et al., 2010). Transcription-level fluctuation of ethylene receptors during flowering was reported in tree peony (*Paeonia suffruticosa*; Zhou et al., 2010). Phytochrome activity is also involved. Kaihara and Takimoto (1980) demonstrated that a flash of red light during the night before anticipated floral opening can alter the time of floral opening on the following day. The effect of red light was diminished by a subsequent exposure to far-red light. MicroRNA regulation of flower opening was proposed after comparing microRNA levels between buds and flowers in 5-year-old plum blossom trees (*Prunus mume*; Wang et al., 2014). Nevertheless, the regulatory network that oversees transcription alteration remains unclear (van Doorn and Kamdee, 2014). Few mutants specific to floral opening have been identified in model plant systems (van Doorn and Kamdee, 2014); a mutation in a RINGv E3 ubiquitin ligase that causes reduced cutin biosynthesis or loading was found to cause a lack-of-opening phenotype in oilseed rape (*Brassica napus*), suggesting the critical role of cutin in successful floral opening

(Lu et al., 2012). Only one forward genetic study has investigated the genetic regulation of floral opening time (Nitta et al., 2010); the segregation of morning flowering versus evening flowering in an F_2 population derived from a hybrid between daylily (*Hemerocallis fulva*) and night lily (*H. citrina*) suggested the presence of a major effect gene. This study also suggested independent regulation of floral opening and closure times in lily.

In order to understand more about the genetic regulation of floral opening time, we analyzed natural variation in this phenotype in *Lactuca serriola* (wild lettuce) and *L. sativa* (lettuce). *Lactuca* spp. are members of the Compositae family with compound hermaphrodite inflorescences that only open once. *L. serriola* is the wild progenitor of modern cultivated lettuce and is fully reproductively compatible with *L. sativa*. We took advantage of a recombinant inbred line (RIL) population developed from a cross between accessions of *L. serriola* and *L. sativa* that differed for floral opening time by 3.5 hours. We overcame the challenge of studying floral opening time in a large, replicated RIL population by utilizing drones equipped with a multi-spectral camera to repeatedly image the entire experimental field. Effectiveness of drones in high-throughput crop phenotyping has been demonstrated in recent studies (Spindel et al., 2018; Xu et al., 2019). In our study, data from hourly drone flights were analyzed using an innovative combination of machine learning and Bayesian statistics to quantify the floral opening phenotype. Two significant quantitative trait loci (QTLs) collectively explained more than 30% of the phenotypic variation of floral opening time; these QTLs contained genes known to regulate circadian rhythms in Arabidopsis.

Results

Most lettuces, including the oil seed type PI251246, start to flower early in the morning. In contrast, *L. serriola* accession Armenian999 does not flower until the afternoon. Two-hundred and thirty-six F_6 RILs that had been developed from crossing these two accessions were available for investigating the genetic basis of asynchronous floral opening phenotype. This phenotype is illustrated in a short video made using time lapse photography of two RILs from this population (https://www.youtube.com/watch?v=9w8iRTHXBxM) taken from an experimental field in Davis, CA, in June 2014, which corresponds to a 3-hour span in real time. In this video, flowers of one RIL begin to open approximately 55 minutes before the other. This segregating phenotype is also illustrated by photographs of individual flowers taken over an 8-hour time span of four RILs and the parents grown in a screenhouse in Davis, CA in June 2020 (Figure 1).

Remote sensing phenotyping

The 236 RILs, both parental lines, and two controls, *L. sativa* cv. Salinas and *L. serriola* accession US96UC23, were planted in two complete randomized replicates of eight plants in Davis, CA, during summer 2019. Multi-spectral images were captured at 9 am, 11 am, 1 pm, and 3 pm on July 1st, 2019, and 10 am, 12 pm, 2 pm, and 4 pm on July 9th using a multispectral camera mounted on a drone. Each drone flight took an average of nine minutes. On average, 2,309 raw images with 85% front- and side-overlap were generated per flight. The 2 pm drone flight did not generate any images due to technical errors and had to be discarded. A total of seven whole-field images at 1 cm spatial resolution were generated by GPS-guided tiling of raw images. Yellow floral pixels are visible to the naked eye from whole-field images (Figure 2 and Supplementary Figure S1).

Machine learning classification of floral pixels

A total of 4,807 floral, vegetative, and ground pixels were randomly sampled from the super-high-resolution field images at all seven time points (Supplementary Table S1). Pairwise scatterplots of the Hue-Saturation-Value (HSV) values of the sample pixels indicated clear distinction between pixels belonging to different categories (Figure 3a). Images taken at different time points appeared to be largely homogeneous regarding pixel HSV (Figure 3b).

Machine learning was used to classify pixels from whole-field images into "floral," "vegetative," or "ground" categories. The 4,807 labeled sample pixels were divided evenly into a training dataset (2,404 samples) and a testing dataset (2,403 samples). Five machine learning algorithms were trained using the training dataset. Ten-fold cross-validation test of pixel classification accuracy showed that the support vector machine (SVM) model outperformed all other models with a mean classification accuracy of 99.15%. When used to classify pixels in the testing dataset, the SVM model made predictions with 99.08% accuracy (Table 1 and Figure 4b). A final SVM model was trained using all sample pixels and tuning hyperparameters sigma = 1.102 and C = 0.5. The final model produced a total of 308 support vectors and had within-sample prediction accuracy of 99.12%.

The final SVM model was deployed to predict floral pixels in all field images. Plot-level floral pixel counts at all seven time points are listed in Supplementary Table S2. The total number of predicted floral pixels ranged from 2,730 at 4 pm to a daily maximum of 1,395,676 at 11 am. The change in the total number of floral pixels throughout the course of the day peaked in the late

161 morning, consistent with maximum floral opening on a population level being between 11 am and
162 12 pm (Figure 5).
163
164 *Bayesian inference of peak floral opening time*
165 The peak floral opening time (FOT) of individual plots was inferred from the hourly floral pixel
166 count for each plot. Figure 6 is a visualization of the output of SVM floral pixel classification. Plot
167 "1" in the blue box clearly reached peak opening early in the day, near 10 am. Similarly, plot "2"
168 in the green box had peak FOT near 11 am, plot "3" (yellow box) near 12 pm, and plot "4" (orange
169 box) near 1 pm (Figure 6). The temporal increase and decrease of the floral pixel count throughout
170 the course of a day within each plot can be described using a distinct bell-shaped curve, with
171 parameter τ characterizing the peak FOT of the plot, i.e., the mean and mode of the curve, and
172 parameter δ^2 characterizing the duration of the opening within the plot.
173
174 A bell-shaped likelihood function with parameters $\{\tau_k, \delta_k^2\}$ that best described the hourly floral
175 pixel fluctuation of plot k (k = 1, 2, …, 480) was fitted to the time-series floral pixel data for each
176 plot using Markov Chain Monte Carlo (MCMC). Divergent incidences were re-fitted by the
177 MCMC to account for possible poor initialization. All plots converged after two iterations of
178 sampling. The inferred peak FOT between the two blocks showed strong correlation ($R^2 = 0.485$;
179 Figure 7, Figure 8, and Supplementary Figure S2). Simple linear regression model reported no
180 significant difference of peak FOT between the two blocks ($p = 0.10$). Therefore, the mean
181 phenotype was calculated using the simple Euclidean mean between the two blocks.
182

Inferred peak FOT ranged from 09:17 am to 1:08 pm, following a slightly heavy-tailed normal distribution with a mean of 11:29 am (Figure 9; Supplementary table S3). The standard deviation of phenotypic distribution is 36.8 minutes. The inferred peak FOT of the early opening parent, PI251246, was 9:34 am, while that of the late opening parent, Armenian999, was 1:15 pm. No obvious transgressive segregation was found within the population.

Genotyping

A total of over 354 million 100 bp Illumina reads were obtained from all RILs. Mapping reads to version 8 of the lettuce reference genome (Reyes-Chin-Wo et al., 2017) yielded 422,418 single nucleotide polymorphism (SNP) markers, covering all nine chromosomes of the lettuce genome. After filtering against missing data and segregation distortion, 18,805 SNP markers remained. LepMap3 (Rastas, 2017) was used to produce a genetic map comprising 17,402 SNP markers in 2,677 genetic bins, covering 1,883 cM in the nine chromosomal linkage groups (Supplementary Figure S3), which is similar to the previously reported genetic map size (Truco et al., 2013). The heterozygosity rate of selected SNPs was 3.25%, consistent with the expected heterozygosity rate for F_6 populations, 3.13%. No regions exhibited severe segregation distortion. One SNP marker was selected from each genetic bin, resulting in 2,677 markers for QTL mapping. The mean distance between each pair of adjacent markers is 0.7 cM. Four gaps larger than 5 cM are present in this map; these gaps are located at 149.0–155.8 cM on linkage group 3, 155.8–166.2 cM on linkage group 3, 62.8–68.1 cM on linkage group 7, and 50.3–55.7 cM on linkage group 9. Four RILs were excluded from downstream analyses due to the large percentage of missing genotype data, resulting in a final set of 232 RILs for QTL mapping.

206 *QTL analysis*

207 Genotype and peak FOT phenotype data for 232 RILs were used for QTL mapping. Mixed effect
208 modeling estimated the narrow sense heritability of the phenotype to be 0.8765. The significance
209 threshold of the permutation test was set at negative log of odds (LOD) = 3.14 for the type I error
210 rate of 0.05. Two significant QTLs were identified for peak FOT on Chromosomes 2 (LOD = 10.3)
211 and 8 (LOD = 7.7) (Figure 10). The physical location of flanking markers and summary statistics
212 of the effects of the two QTLs are detailed in Table 2. In both QTLs, the allele from the late-
213 flowering parent, Armenian999, contributed to the later flowering phenotype (Figure 11).

214

215 *Candidate genes*

216 The two significant QTLs, *qDFO2.1* (*Daily Floral Opening on chromosome 2)* and *qDFO8.1*,
217 were investigated for candidate genes of known function in Arabidopsis. There are 309 gene
218 models located within 1 LOD score on each side of the peak of *qDFO2.1* and 123 gene models
219 within *qDFO8.1* in the reference annotation (Reyes-Chin-Wo et al., 2017). Among these 432 genes,
220 199 had coding sequence variants between the parents (Supplementary Table S4). Of the 1,752
221 orthologs of Arabidopsis genes involved in flowering time and/or circadian clock regulation, five
222 were located within *qDFO2.1*; two of these genes exhibited coding sequence variants (Table 3).
223 No orthologs involved in flowering time and/or circadian clock regulation were identified within
224 *qDFO8.1*.

225

226 **Discussion**

227 Our study demonstrated the efficacy of using drones to detect quantitative temporal differences in
228 floral opening events. We were able to collect multispectral data on a large number of plants

multiple times per day. Machine learning enabled fast, robust recognition of phenotypes. Bayesian approaches provided a summary statistic for flower opening time of each line that was used for QTL analysis. This revealed two significant genomic regions determining floral opening time.

The machine learning algorithm predicted that the floral opening behavior of each single-genotype plot followed a Gaussian-like curve throughout the course of a day (Figure 5). The time-stamped floral pixel count data was then passed down to a Bayesian framework to extract summary statistics for floral opening time. The number of floral pixels captured by a drone image is a function of both the number of opening inflorescences and the degree of their opening (Figure 1). The peak floral opening time reflects the average opening time of all individual inflorescences within a plot. From an analytical standpoint, peak floral opening time is a better summary statistic for the floral opening process than the beginning or ending points because it is readily defined mathematically and is robust against detection errors. A Gaussian-like likelihood function was used to model the floral opening process and a MCMC sampler was used to estimate the peak timepoint. Each RIL had two independently inferred peak floral opening times, from the two blocks of the experiment. The high similarity between replicates verified the robustness of the Bayesian inference protocol. Our method is a hybrid workflow that processes time-stamped high-throughput phenotyping data by feeding raw image data through a machine learning module and a Bayesian inference module in a sequential manner. This modular approach harnesses the respective strengths of the two procedures independently and provides multiple advantages. This flexible workflow can be adapted to different experimental designs and phenotyping goals with only minor changes. Any phenotype that can be scored using time-stamped images could benefit from adopting this workflow with custom likelihood functions based on the biological nature of the phenotype. For

252 example, one could readily substitute with a sigmoid likelihood function for modeling for
253 cumulative phenotypes such as plant height and canopy metrics. Another advantage this workflow
254 has over exclusively-machine-learning-based procedures is that the addition of a specified
255 likelihood function results in interpretable models with biologically meaningful parameters
256 suitable for downstream analyses.
257
258 The timepoint at which each RIL reaches peak floral opening varied from early morning to early
259 afternoon in a continuous fashion during the days that the RILs were flowering (Figure 9). QTL
260 mapping identified two loci significantly associated with floral opening time. Each allele from the
261 late flowering parent Armenian999 on the two QTLs contributed additively to a later floral opening
262 phenotype (Figure 11). In contrast to the extensively studied initiation of flowering, floral opening
263 time has been little studied (van Doorn and van Meeteren, 2003; van Doorn and Kamdee, 2014)
264 and not to the locus level (Nitta et al., 2010). This study reports the first genetic loci associated
265 with the regulation of floral opening time.
266
267 The largest effect QTL, qDFO2.1, collocates with a QTL that is associated with multiple bolting,
268 budding and flowering time traits in lettuce (Lavelle, 2009). Two genes within qDFO2.1 with non-
269 synonymous variants between the parents have been shown to be involved in the regulation of the
270 circadian clock and initiation of flowering in Arabidopsis (Table 3); these include an ortholog to
271 Arabidopsis UBIQUITIN SPECIFIC PROTEASE 12 (UBP12) and UBP13. *At*UBP13 and
272 *At*UBP12 are ubiquitin-specific proteases capable of rapid, posttranslational regulations of diverse
273 cellular processes in Arabidopsis (Cui et al., 2013). The other candidate gene within qDFO2.1 is
274 orthologous to Arabidopsis CHC1 (alternatively known as BAF60), which is involved in

transcriptional activation and repression of flowering regulation genes by chromatin remodeling (Jégu et al., 2014). The absence of floral initiation or circadian clock orthologs within qDFO8.1 suggests that there are separate regulatory mechanisms for floral opening time besides these well studied pathways. The two loci identified in this study provides the foundation for future experiments focused on causal gene identification and functional validation.

The timing of floral opening critically impacts a plant's survival and reproduction in its community (Kehrberger and Holzschuh, 2019). Our study identified two genetic loci determining natural variation in the regulation of floral opening time in lettuce. This raises the question of the evolutionary pressures for diversity in the trait. Variation in floral opening time may be important in synchronizing floral opening with maximum activity of local pollinators. Thermal constraints on flight activity may limit the pollinating effectiveness of insects; each species of pollinating insect has a microclimatic window within which foraging flight can be sustained (Corbet et al., 1993). The late-blooming parent of the mapping population, Armenian999, is an *L. serriola* accession collected from the cold, wet mountain area of Armenia. In contrast, the early-blooming parent, PI251246, is a landrace accession originating in Egypt. The differential floral opening habits might therefore have evolved in adaptation to different pollinator activities in their respective native environments as has been shown for *Saxifraga oppofitifolia* in alpine elevations (Gugerli, 1998). It would be interesting to investigate whether there is a correlation between floral opening time of diverse lettuce accessions and the climate of their native habitats.

In this study, the combination of machine learning image processing and Bayesian modeling was proved to be highly effective in processing and analyzing time-series aerial images of the field

298 experiment. This versatile framework can be readily adapted to other projects aiming to take
299 advantage of the speed and mobility of drone imaging technologies. Customization in our
300 workflow in choosing suitable machine learning algorithms and Bayesian likelihood functions can
301 enable detection and modeling of phenotypes on the time dimension in other areas such as ecology
302 and population genetics.
303
304 **Methods**
305 *Time lapse video and photography*
306 The video was generated with shots at 3 second intervals (3,600 intervals in total), taken with a
307 Canon G15 camera using Canon Hack Development Kit intervalometer script
308 (http://chdk.wikia.com/wiki/CHDK) on June 7th, 2014 in the field at Davis, CA. Individual photos
309 were compiled into 30 fps movie clip using PhotoLapse 3 (Version 1.0, S. van der Palen;
310 http://home.hccnet.nl/s.vd.palen/). Close-up photographs of flowers of four asynchronously
311 flowering RILs of the Armenian999 x PI251246 RIL population and the parents were taken at 1-
312 hour intervals on June 7th, 2020 using a Canon EOS 50D DSLR Camera. The photographed plants
313 were grown in a screenhouse in Davis, CA.
314
315 *Mapping population and field design*
316 Two-hundred and thirty-six F_6 RILs had been developed from crossing the *L. serriola* accession
317 Armenian999 with the *L. sativa* landrace PI251246 (M.-J. Truco, unpublished). The 236 RILs,
318 both parental lines, and two controls, *L. sativa* cv. Salinas and *L. serriola* accession US96UC23,
319 were grown in summer 2019 at the Department of Plant Sciences field facility in Davis, CA. The
320 plants were seeded on May 6th, 2019 and transplanted into 40-inch-wide raised beds in the field on

June 5th, 2019. Each raised bed consisted of two rows; every other bed was left empty to allow field access throughout the growing season. The experiment had two complete randomized blocks, each consisting of 240 plots to accommodate the 240 genotypes. Within each block, eight individuals of each RIL or parent were planted into one 10 ft x 1 row plot. The blocks were arranged along the direction of the furrow irrigation system to control for variations attributable to water availability.

Weather data

Weather data for the dates of the drone flights were collected from the National Centers for Environmental Information website (https://www.ncdc.noaa.gov/) for the University Airport, CA weather station (Station ID WBAN:00174, GPS coordinates 38.533°, -121.783°). The weather station was less than 500 m away from the farthest corner of the experimental field.

Phenotyping by remote sensing

Seven ground control points were set up in the field, four near the corners and three along the field's East–West centerline. GPS coordinates, with an accuracy within a few centimeters, were recorded using a handheld data collector (Trimble Geo 7x Series, Trimble Inc., Sunnyvale, CA). These coordinates were used in processing drone images to ensure that images collected at different times and dates aligned perfectly with one another.

A MicaSense RedEdge multi-spectral camera was mounted on a DJI Matrice100 drone. The camera captured images at five wavelengths: blue (475 nm center, 20 nm bandwidth), green (560 nm center, 20 nm bandwidth), red (668 nm center, 10 nm bandwidth), red edge (717 nm center, 10

nm bandwidth), and near-infrared (840 nm center, 40 nm bandwidth). In this study, only the blue, green, and red wavelengths were used for flower identification. The drone was flown over the experimental field at 9 am, 11 am, 1 pm and 3 pm on July 1st, 2019, and 10 am, 12 pm, 2 pm and 4 pm on July 9th, 2019. The sky was cloudless on both days; daily minimum and maximum temperatures were 13.9°C–31.1°C and 13.9°C–28.9°C; sunrise was at 5:46 am and 5:50am, respectively. A DJI GS Pro app was used to plan and execute the flight. The drone flew at 15 m above ground, and images were taken at a frequency that ensured 85% front- and side-overlaps between each pair of adjacent images. A MicaSense calibration panel was used for automated adjustment of the reflectance spectra. Raw images from the camera were stitched and processed with the Pix4DMapper Pro photogrammetry software to generate orthomosaic maps of surface reflectance at 1 cm spatial resolution. On average, 2,309 raw images were generated per time point, and 2,181 raw images were used to assemble each five-spectrum field map. With the reconstructed maps, the borders of individual plots were manually determined using the software ArcMap.

Machine learning classification of floral pixels

In order to train a machine learning model that could accurately identify floral pixels from a field image, pixels of flowers, vegetative bodies, and bare ground were randomly sampled and manually labeled from all images based on visual interpretation. A total of 1,569 floral pixels, 1,681 vegetative pixels, and 1,557 ground pixels were labeled (Supplementary Table S1). The HSV values of the sampled pixels were extracted. Half of the pixels (2,404) were randomly selected to be used to train five machine learning models, linear discriminant analysis, k-nearest neighbor, SVM, random forest, and classification and regression tree, using R package “caret” (Kuhn, 2008), for floral pixel identification. A 10-fold within-sample cross-validation test and an out-of-sample

validation test with the remaining half of the HSV dataset were performed to compare the prediction accuracy of the machine learning models.

The best performing machine learning model, the SVM model, was trained using HSV values of all 4,807 sampled pixels and used to predict floral pixels for all field images. Once the coordinates of all predicted floral pixels were determined, field images were reconstructed to reflect the floral state of each pixel. A polygonal shapefile delineating the borders of all plots was superimposed on the reconstructed field images to extract the floral pixel counts within each of the 480 plots at each time point. Each plot's daily maximum floral pixel count was calculated and the plot-level floral pixel counts were normalized by dividing the count number at each time point by the plot daily maximums.

Bayesian inference of peak floral opening time

A Gaussian-like likelihood function was used to describe the fluctuation of plot-level floral pixel counts of plot *k* ($Y_{k,t}$, $k = 1, 2, ..., 480$) at any given time point (t) throughout the course of a day:

$$Y_{k,t} = e^{-\frac{(t-\tau_k)^2}{2\delta_k^2}} + \varepsilon_{k,t}$$

$$\varepsilon_{k,t} \sim N(0, \sigma^2)$$

The function peaks at Y = 1 when $t = \tau_k$. τ_k is the center of the symmetric, bell-shaped curve; it describes the time point at which plot *k* reaches its daily global maximum floral opening. Another parameter, δ_k^2, determines the spread of the curve, and hence describes the duration of floral opening in plot *k*.

The following weakly regularizing priors were chosen:

$$\tau_k \sim N(12, 1)$$

$$\delta_k^2 \sim \exp(1)$$

$$\sigma^2 \sim \exp(1).$$

Four 2,000-iteration Markov Chain Monte Carlo (MCMC) were used to sample from the posterior distributions of τ_k, δ_k^2, and σ^2 using R package "rethinking" (McElreath, 2016). After 2,000 sampling iterations, plots whose MCMC for τ had effective sample sizes below 50 were fed through the modeling pipeline for a second iteration to account for possible poor fitting due to suboptimal initialization. Point estimate of the posterior distribution of τ_k, $\hat{\tau}_k$, was used as estimated peak FOT for plot *k*. Block effect was assessed using fixed effect simple linear regression. The Euclidian mean between the peak FOTs of the two replicates were used as the phenotypic values for genetic mapping.

Genotyping and QTL analysis

For DNA extraction, approximately 30 seeds per genotype were placed in a 2 mL Eppendorf Safe Lock tube along with one stainless steel bead (Qiagen Cat. No. 69989), frozen in liquid nitrogen, and ground to a powder in a Qiagen TissueLyser. Seven hundred microliters of 5 M guanidine thiocyanate in 20 mM Tris-HCL (pH 6.75) was added to tissue powder, vortexed until homogenized and spun in microcentrifuge (RT) for 5 min at 14,000–20,000 g. After centrifugation, 600 µL of clear lysate was transferred to DNA binding plates (Epoch Life Sciences EconoSpin™

96 well) stacked over a 1 mL collection plate and centrifuged 5 minutes (RT) at 1,300 g. Flow through was discarded. DNA binding plate was incubated with 600 µL of liquid for 4 minutes at RT and centrifuged at 1,300 g for 5 minutes sequentially with PB buffer (Qiagen Cat. No. 19066), followed by PE buffer (Qiagen Cat. No. 19065), and then with two 80% EtOH washes. DNA plate was dried in centrifuge over paper towels for 5 minutes at 2,000 g. DNA was eluted from binding plate into new collection plate after 5-minute incubation in 60 µL of 10 mM Tris-HCL (pH 8.0) at 65°C. DNA was quantified using Qubit. DNA from parental lines and segregating individuals was digested using *AvaII* to reduce the genome complexity of the samples (Sandoya et al., 2019). Individual samples were barcoded, pooled, and genotyped by sequencing using paired-end 100 bp Illumina HiSeq4000. The parental lines, Armenian999 and PI251246, were also whole-genome-shotgun sequenced using paired-end 150 bp and 100 bp Illumina HiSeq4000 to 29x and 17x coverages, respectively. Sequencing results were de-multiplexed using GBSX software in the demultiplex mode (Herten et al., 2015). All reads were mapped to the *L. sativa* reference genome v8.0 (Reyes-Chin-Wo et al., 2017) using bwa-mem (Li, 2013) and variants were called using FreeBayes (Garrison and Marth, 2012). SNPs called against the reference that were polymorphic between the two parental lines with a quality score greater than 20 and with fewer than 20% missing data across all RILs were used to construct a genetic map using the software LepMap3 with 20 cM as the cutoff threshold for linkage groups and the significance level at p-value = 10^{-6}. One representative SNP from each genetic bin was selected for QTL mapping. Linkage group numbers were determined by the chromosomal location of the markers relative to the reference genome. Heritability of the phenotype was estimated using mixed effect modeling with R packages "synbreed" (Wimmer et al., 2012) and "sommer" (Covarrubias-Pazaran, 2016) using block-level phenotype data. QTL analysis was performed using 2,677 SNP markers, each representing distinct

436 genetic bins. The R package "qtl" was used for interval mapping, 10,000-iteration permutation test,
437 and QTL effect analysis (Broman et al., 2003).
438
439 *Candidate gene identification*
440 Single nucleotide variants, insertions, deletions, stop-loss variants and stop-gain variants were
441 identified between the parental lines using software ANNOVAR (Wang et al., 2010). Genes were
442 filtered for non-synonymous variations in coding sequence between the parental lines. Orthofinder
443 (Emms and Kelly, 2015) was used for genome-wide prediction of lettuce orthologs of *Arabidopsis*
444 *thaliana* genes.
445
446 **Acknowledgements**
447 We thank J. Emerson for greenhouse and field assistance, A. Vargas for DNA and GBS library
448 construction, D. Feinberg for assistance with raw image processing, and H. Xu for data submission
449 to NCBI Sequence Read Archive (SRA) database. This research was funded by an NSF Graduate
450 Research Fellowship to RH and a USDA NIFA Specialty Crop Research Initiative (SCRI) Grant #
451 2015-51181-24283 to RWM.
452
453 **Data Availability**
454 GBS data of the RILs and WGS data of the parents are available on the NCBI SRA database under
455 BioProjects PRJNA642889, PRJNA510128, and PRJNA478460, respectively. Scripts used in the
456 study for machine learning and Bayesian inference are available on GitHub at
457 https://www.github.com/rkbhan/FloralOpening. GPS-anchored aerial image data are available on
458 HydroShare at https://www.hydroshare.org/resource/1c5855dbeb3c49a8b5779300550e08f1/.

Tables

Table 1. Prediction accuracy of support vector machine algorithm, checked using testing dataset

	Testing: floral	Testing: vegetative	Testing: ground
Prediction: floral	792	1	4
Prediction: vegetative	3	779	8
Prediction: ground	7	6	803

Table 2. QTL linked to differential floral opening hour (*qDFO*) and their effects

QTL	1-LOD interval Physical Location (Base)	1-LOD interval Genetic Location (cM)	LOD	p-value	Variance Explained	Effect of AA allele (hours)
qDFO2.1	Chr2: 183,906,862–190,964,979	LG2: 148.7-159.0	10.3	0	18.23%	0.48
qDFO8.1	Chr8: 196,253,927–202,987,597	LG8: 153.4-156.9	7.7	0	13.84%	0.4

Table 3. Candidate genes within QTL *qDFO2.1* with non-synonymous variations between parents and orthology to Arabidopsis genes involved in flowering time and/or circadian clock regulation.

Lettuce gene model name	Variant type*	Arabidopsis ortholog
Lsat_1_v5_gn_2_94800	NS-SNV	*BAF60; CHC1*
Lsat_1_v5_gn_2_93700	NS-SNV, FS-Del, NFS-Ins, NFS-Sub	*UBP12, UBP13*

*Variant types: “NS-SNV”: non-synonymous single nucleotide variant; “FS-Del”: Frameshift deletion; “NFS-Ins”: non-frameshift insertion; “NFS-Sub”: non-frameshift substitution.

References

Broman KW, Wu H, Sen Ś, Churchill GA (2003) R/qtl: QTL mapping in experimental crosses. Bioinformatics **19**: 889–890

Colquhoun TA, Schwieterman ML, Wedde AE, Schimmel BCJ, Marciniak DM, Verdonk JC, Kim JY, Oh Y, Gális I, Baldwin IT, et al (2011) EOBII Controls Flower Opening by Functioning as a General Transcriptomic Switch. Plant Physiol

156: 974 LP – 984

Corbet SA, Fussell M, Ake R, Fraser A, Gunson C, Savage A, Smith K (1993) Temperature and the pollinating activity of social bees. Ecol Entomol **18**: 17–30

Covarrubias-Pazaran G (2016) Genome-Assisted Prediction of Quantitative Traits Using the R Package sommer. PLoS One **11**: e0156744

Cui X, Lu F, Li Y, Xue Y, Kang Y, Zhang S, Qiu Q, Cui X, Zheng S, Liu B, et al (2013) Ubiquitin-Specific Proteases UBP12 and UBP13 Act in Circadian Clock and Photoperiodic Flowering Regulation in Arabidopsis. Plant Physiol **162**: 897 LP – 906

van Doorn WG, Kamdee C (2014) Flower opening and closure: an update. J Exp Bot **65**: 5749–5757

van Doorn WG, van Meeteren U (2003) Flower opening and closure: a review. J Exp Bot **54**: 1801–1812

Emms DM, Kelly S (2015) OrthoFinder: solving fundamental biases in whole genome comparisons dramatically improves orthogroup inference accuracy. Genome Biol **16**: 157

Garrison E, Marth G (2012) Haplotype-based variant detection from short-read sequencing. arXiv Prepr. arXiv1207.3907

Gugerli F (1998) Effect of elevation on sexual reproduction in alpine populations of Saxifraga oppositifolia (Saxifragaceae). Oecologia **114**: 60–66

Harada T, Torii Y, Morita S, Onodera R, Hara Y, Yokoyama R, Nishitani K, Satoh S (2010) Cloning, characterization, and expression of xyloglucan endotransglucosylase/hydrolase and expansin genes associated with petal growth and development during carnation flower opening. J Exp Bot **62**: 815–823

Herten K, Hestand MS, Vermeesch JR, Van Houdt JKJ (2015) GBSX: a toolkit for

493 experimental design and demultiplexing genotyping by sequencing experiments. BMC
494 Bioinformatics **16**: 73
495 **Jégu T, Latrasse D, Delarue M, Hirt H, Domenichini S, Ariel F, Crespi M, Bergounioux C,**
496 **Raynaud C, Benhamed M** (2014) The BAF60 Subunit of the SWI/SNF Chromatin-
497 Remodeling Complex Directly Controls the Formation of a Gene Loop at
498 FLOWERING LOCUS C in Arabidopsis
499 Plant Cell **26**: 538 LP – 551
500 **Kaihara S, Takimoto A** (1980) Studies on the light controlling the time of flower-opening in
501 Pharbitis nil. Plant Cell Physiol **21**: 21–26
502 **Kehrberger S, Holzschuh A** (2019) How does timing of flowering affect competition for
503 pollinators, flower visitation and seed set in an early spring grassland plant? Sci Rep **9**:
504 15593
505 **Kuhn M** (2008) Building Predictive Models in R Using the caret Package. J Stat Software; Vol
506 1, Issue 5 . doi: 10.18637/jss.v028.i05
507 **Lavelle D** (2009) Genetics of Candidate Genes for Developmental and Domestication-Related
508 Traits in Lettuce. University of California, Davis
509 **Li H** (2013) Aligning sequence reads, clone sequences and assembly contigs with BWA-MEM.
510 arXiv Prepr. arXiv1303.3997
511 **Lu Y-H, Arnaud D, Belcram H, Falentin C, Rouault P, Piel N, Lucas M-O, Just J, Renard**
512 **M, Delourme R** (2012) A dominant point mutation in a RINGv E3 ubiquitin ligase
513 homoeologous gene leads to cleistogamy in Brassica napus. Plant Cell **24**: 4875–4891
514 **Matsumoto T, Yasumoto AA, Nitta K, Yahara T, Tachida H** (2013) Difference in flowering
515 time as an isolating barrier. J Theor Biol **317**: 161–167

McElreath R (2016) Statistical rethinking : a Bayesian course with examples in R and Stan.

Nitta K, Yasumoto AA, Yahara T (2010) Variation of flower opening and closing times in F1 and F2 hybrids of daylily (Hemerocallis fulva; Hemerocallidaceae) and nightlily (H. citrina). Am J Bot **97**: 261–267

Rastas P (2017) Lep-MAP3: robust linkage mapping even for low-coverage whole genome sequencing data. Bioinformatics **33**: 3726–3732

Reid MS, Evans RY, Dodge LL, Mor Y Ethylene and silver thiosulfate influence opening of cut rose flowers. **114**: 436–440

Reyes-Chin-Wo S, Wang Z, Yang X, Kozik A, Arikit S, Song C, Xia L, Froenicke L, Lavelle DO, Truco M-J, et al (2017) Genome assembly with in vitro proximity ligation data and whole-genome triplication in lettuce. Nat Commun **8**: 14953

Le Roy K, Vergauwen R, Cammaer V, Yoshida M, Kawakami A, Van Laere A, Van den Ende W (2007) Fructan 1-exohydrolase is associated with flower opening in Campanula rapunculoides. Funct Plant Biol **34**: 972–983

Sakamoto RL, Ito M, Kawakubo N (2012) Contribution of Pollinators to Seed Production as Revealed by Differential Pollinator Exclusion in Clerodendrum trichotomum (Lamiaceae). PLoS One **7**: e33803

Sandoya G V, Maisonneuve B, Truco MJ, Bull CT, Simko I, Trent M, Hayes RJ, Michelmore RW (2019) Genetic analysis of resistance to bacterial leaf spot in the heirloom lettuce cultivar Reine des Glaces. Mol Breed **39**: 160

Spindel JE, Dahlberg J, Colgan M, Hollingsworth J, Sievert J, Staggenborg SH, Hutmacher R, Jansson C, Vogel JP (2018) Association mapping by aerial drone reveals 213 genetic associations for Sorghum bicolor biomass traits under drought. BMC Genomics

19: 679

Truco MJ, Ashrafi H, Kozik A, van Leeuwen H, Bowers J, Wo SRC, Stoffel K, Xu H, Hill T, Van Deynze A, et al (2013) An Ultra-High-Density, Transcript-Based, Genetic Map of Lettuce. G3 Genes|Genomes|Genetics **3**: 617 LP – 631

Vergauwen R, Van den Ende W, Van Laere A (2000) The role of fructan in flowering of Campanula rapunculoides. J Exp Bot **51**: 1261–1266

Wang K, Li M, Hakonarson H (2010) ANNOVAR: functional annotation of genetic variants from high-throughput sequencing data. Nucleic Acids Res **38**: e164–e164

Wang T, Pan H, Wang J, Yang W, Cheng T, Zhang Q (2014) Identification and profiling of novel and conserved microRNAs during the flower opening process in Prunus mume via deep sequencing. Mol Genet Genomics **289**: 169–183

Wimmer V, Albrecht T, Auinger H-J, Schön C-C (2012) synbreed: a framework for the analysis of genomic prediction data using R. Bioinformatics **28**: 2086–2087

Xu R, Li C, Paterson AH (2019) Multispectral imaging and unmanned aerial systems for cotton plant phenotyping. PLoS One **14**: e0205083

Zhou L, Dong L, Jia P-Y, Wang W-R, Wang L-Y (2010) Expression of ethylene receptor and transcription factor genes, and ethylene response during flower opening in tree peony (Paeonia suffruticosa). Plant Growth Regul **62**: 171–179

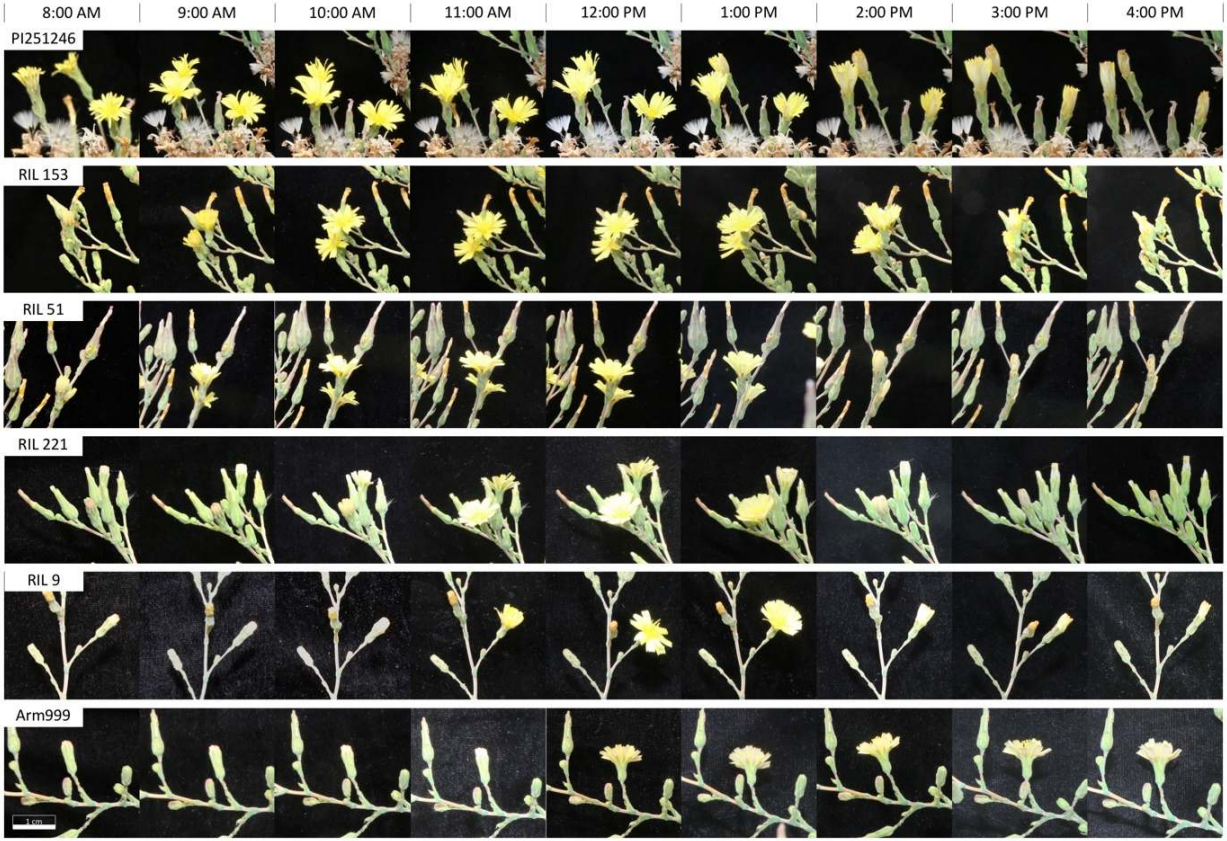

Figure 1. Close-up photographs taken at hourly intervals from 8.00 am to 4.00 pm illustrating the asynchronous floral opening and closing of the parental lines and four RILs of the PI251246 x Armenian999 F_6 population.

Figure 2. Reconstructed field orthomosaic image at 11:00 am on July 1st, 2019. A total of 2,355 raw drone images in five reflectance bands (red, blue, green, red-edge and infrared) were tiled using the Pix4Dmapper Pro software in GPS-guided mode. Only the red, blue and green channels are shown in this figure. The seven ground control points are identified with blue boxes.

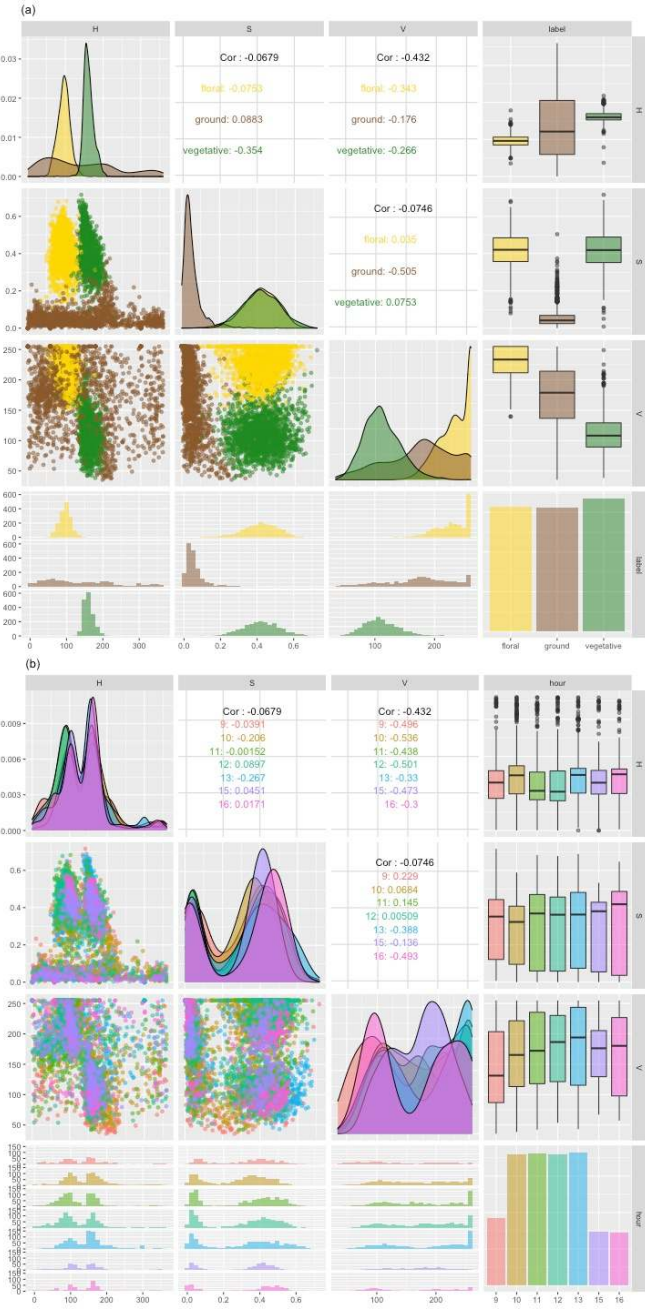

Figure 3. Pair-wise distribution of hue (H), saturation (S) and value (V) of sampled floral (yellow), ground (tan), and vegetative (green) pixels. The plots are colored by pixel labels in (a) and hours in (b). Fewer samples were taken at 9 am, 3 pm and 4 pm due to the small number of floral pixels available at these times. 2(a) demonstrates clear distinction between the three classes of pixels; 2(b) indicates that images taken at different hours of the day are homogeneous in their composition.

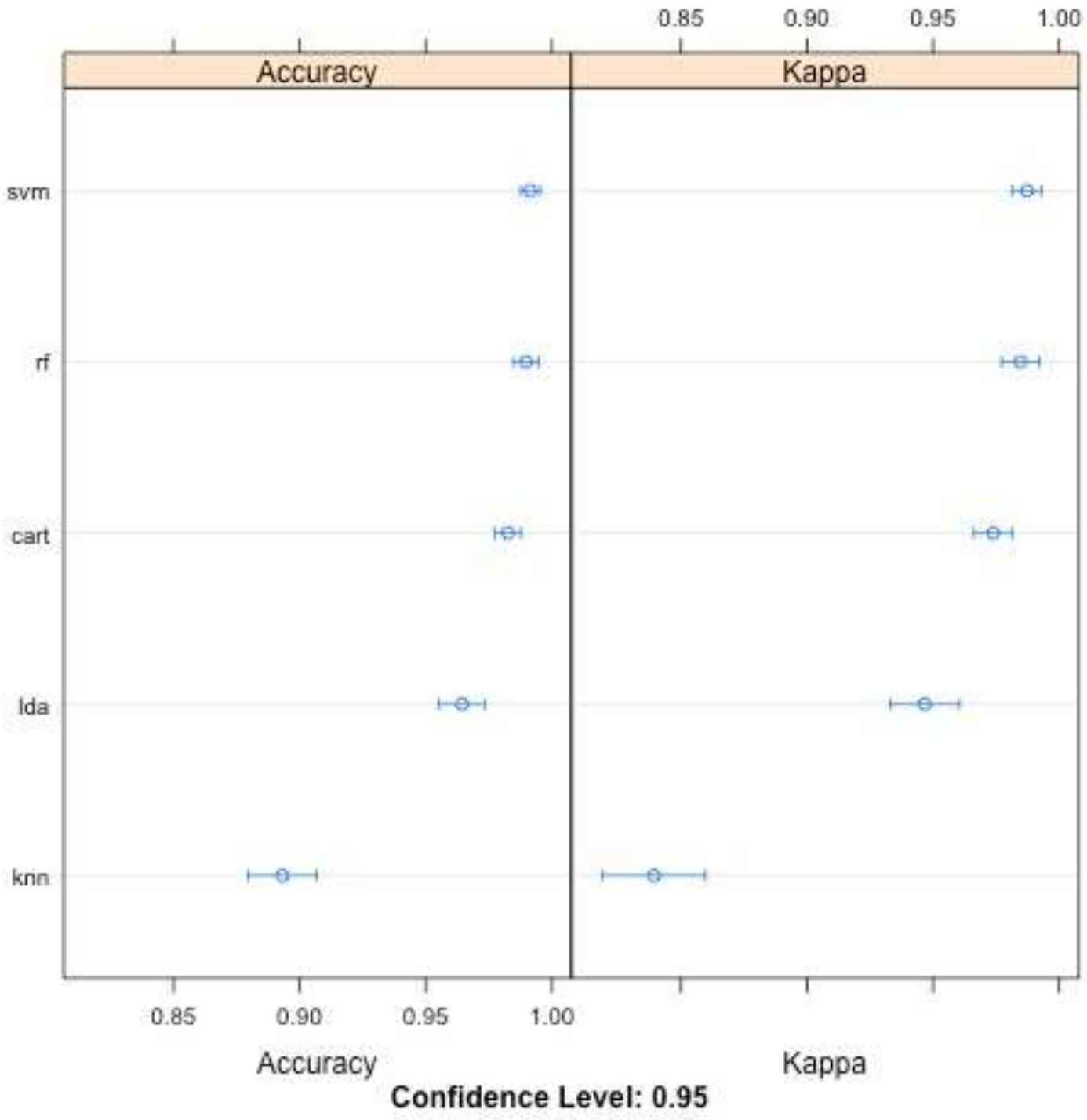

Figure 4. Comparison of pixel classification prediction accuracy and adjusted accuracy ("Kappa") of five machine learning algorithms: support vector machine (SVM), random forest (RF), classification and regression tree (CART), linear discriminant analysis (LDA) and k-nearest neighbors (KNN).

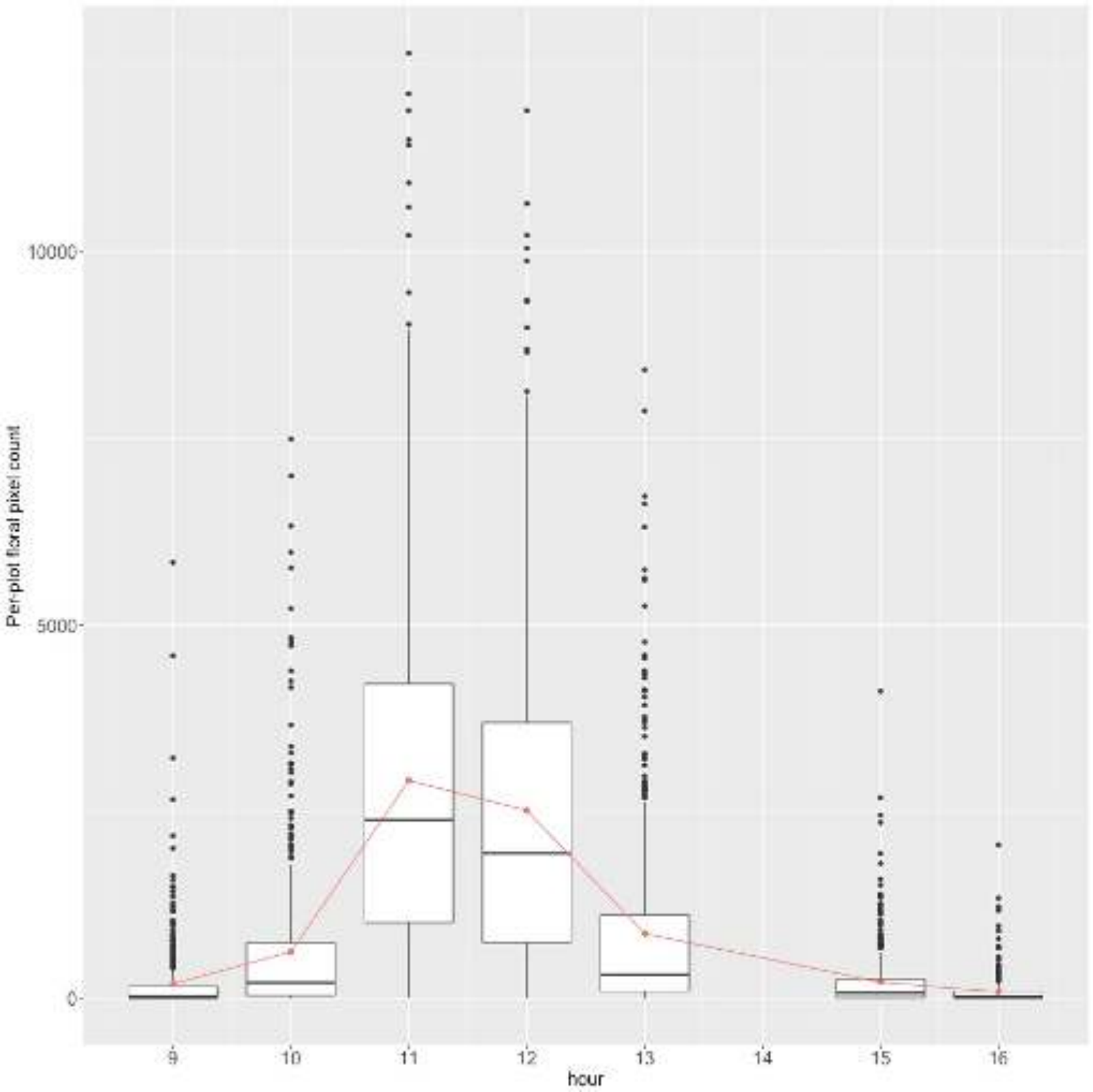

Figure 5. The ranges of per-plot number of floral pixels at each time point. The orange line shows the change of the mean per-plot floral pixel count over time. The box plots show median and quartile of the pixel count distribution at each time point.

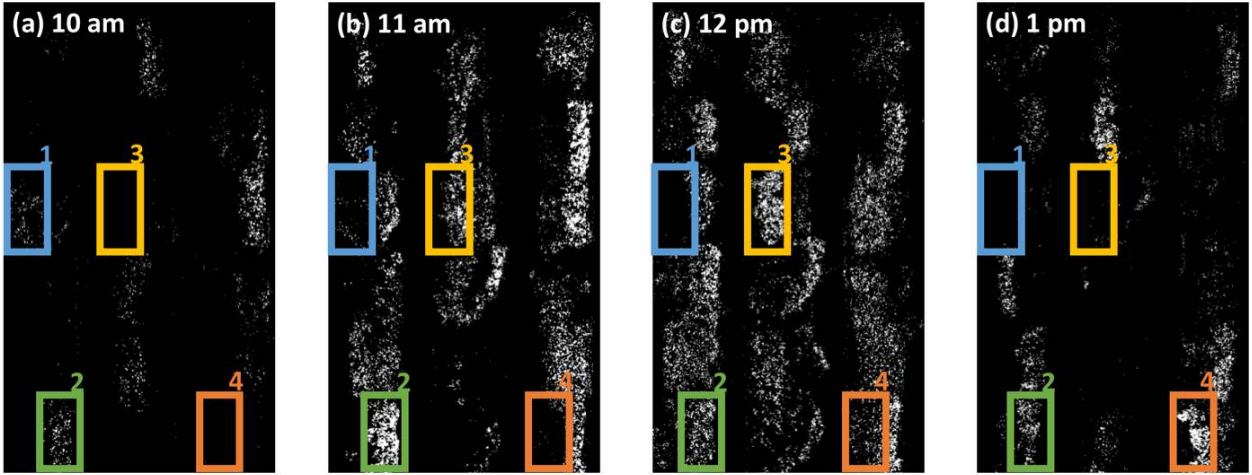

Figure 6. False-colored image of 36 plots based on output of SVM classification of image pixels. Floral pixels were rendered white and non-floral pixels (vegetative or ground) were illustrated in black. Changes in floral pixel count of highlighted plots “1”, “2”, “3”, and “4” through hours (a) 10 am, (b) 11 am, (c) 12 pm and (d) 1 pm show the variation in floral opening time.

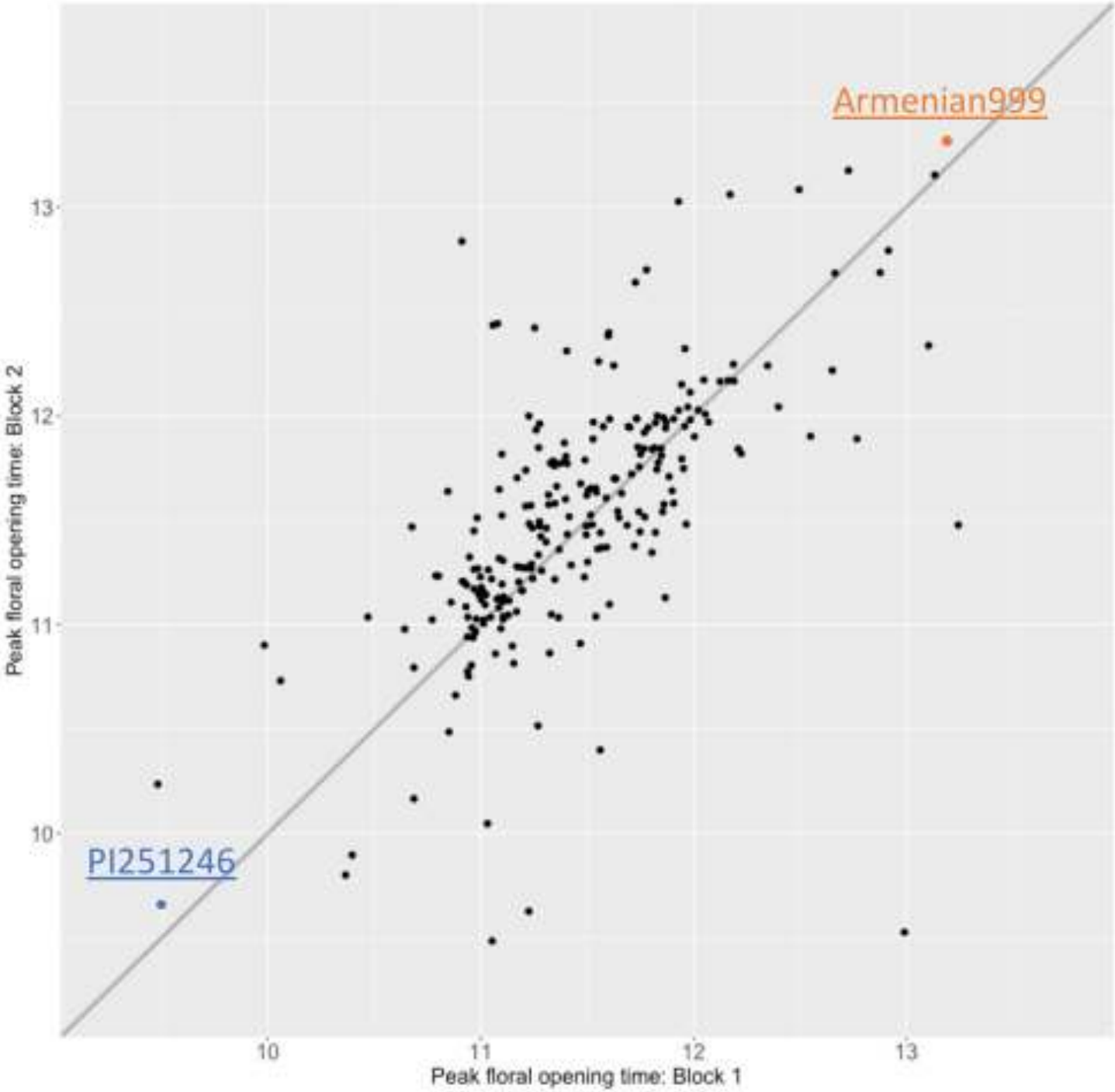

Figure 7. Correlation between-blocks for peak floral opening time of 236 RILs that had a convergent inference and an estimate for both blocks ($R^2 = 0.485$).

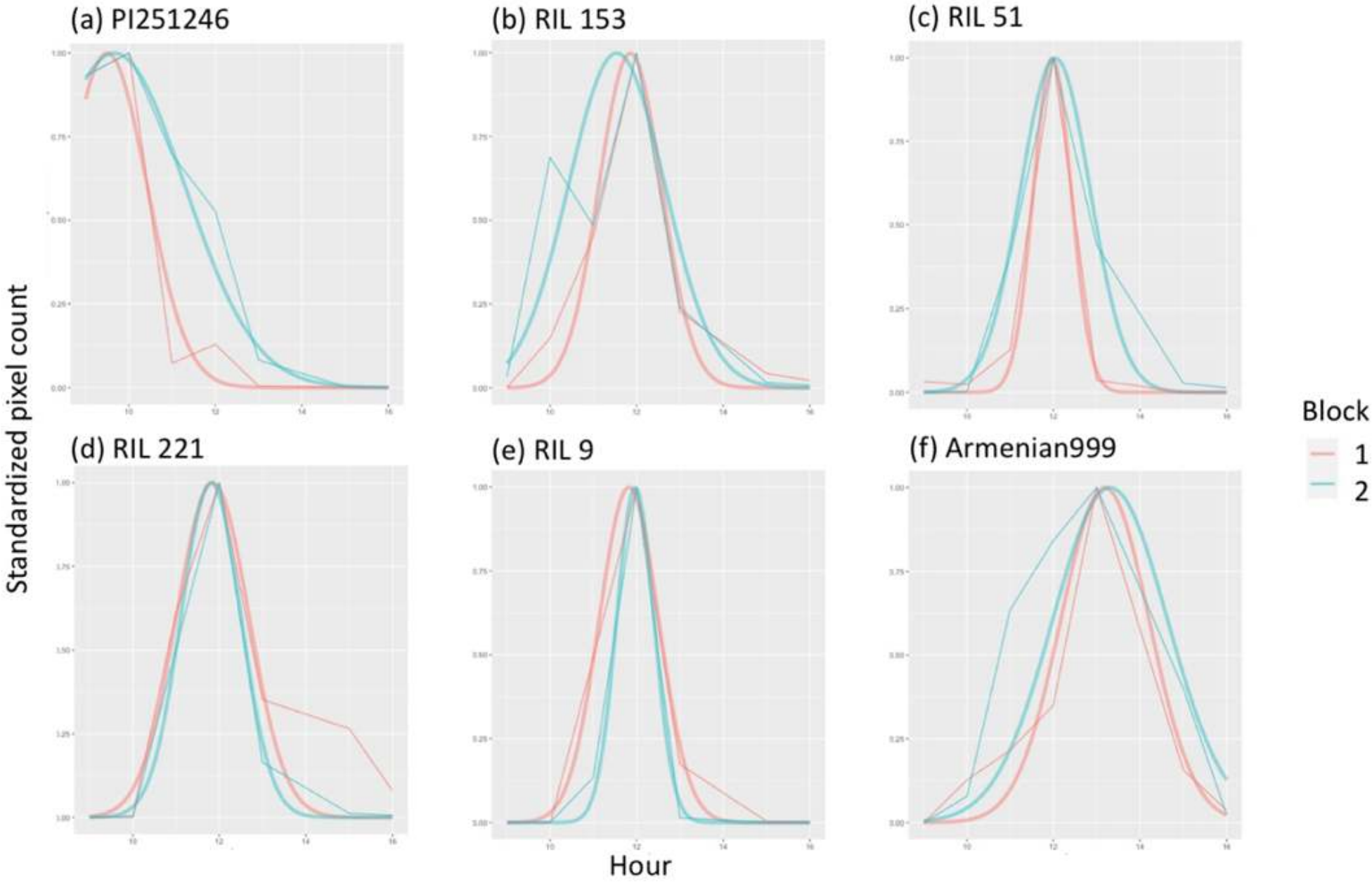

Figure 8. Standardized floral pixel counts for four RILs and the parents throughout the day, overlaid with the respective Bayesian inferred floral opening curve. Close-up photographs of floral opening and closing events of these RILs and the parents are shown in Figure 1.

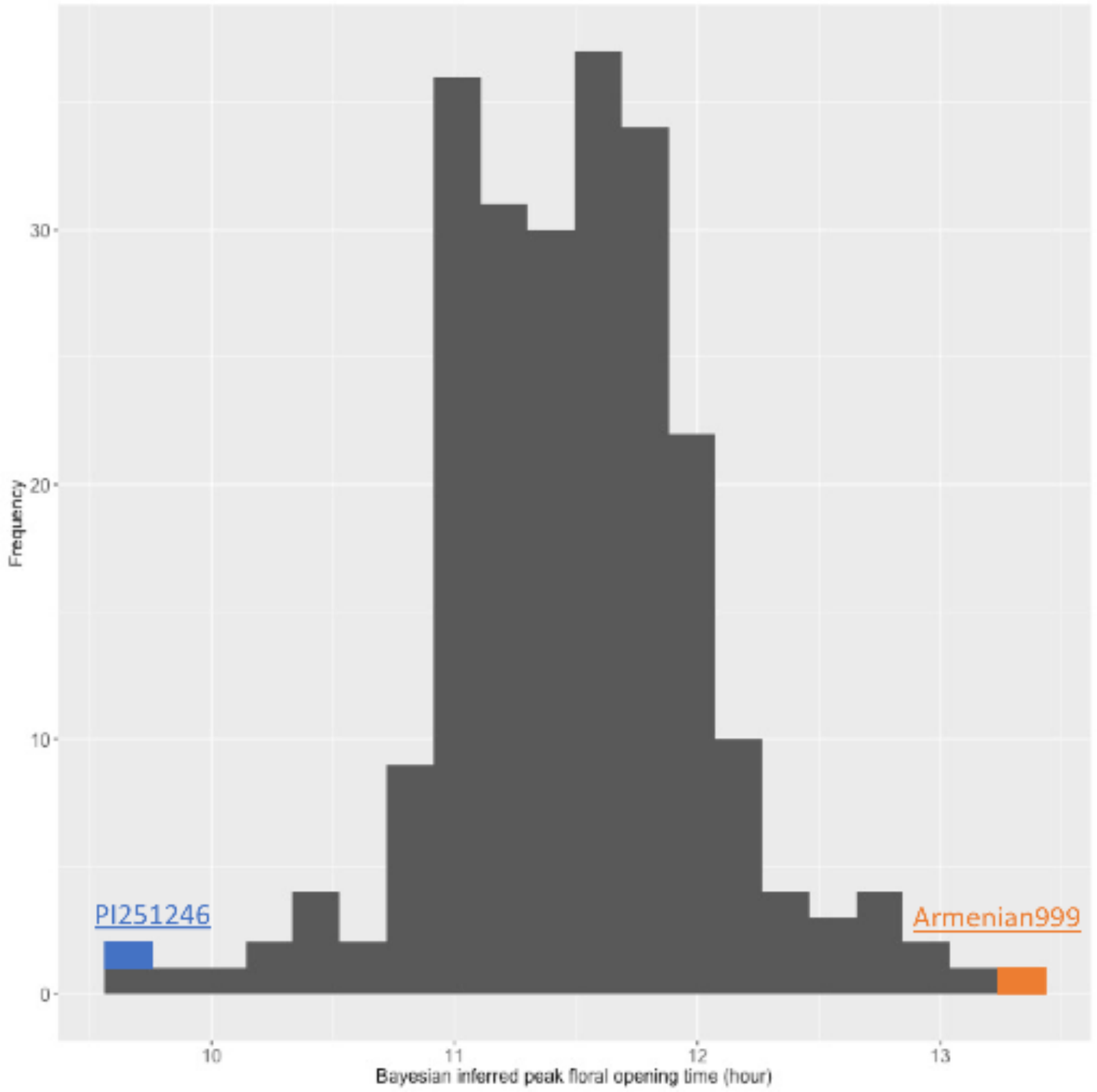

Figure 9. Distribution of high-confidence Bayesian inferred peak floral opening time of the parents and the 236 RILs used in QTL the analysis.

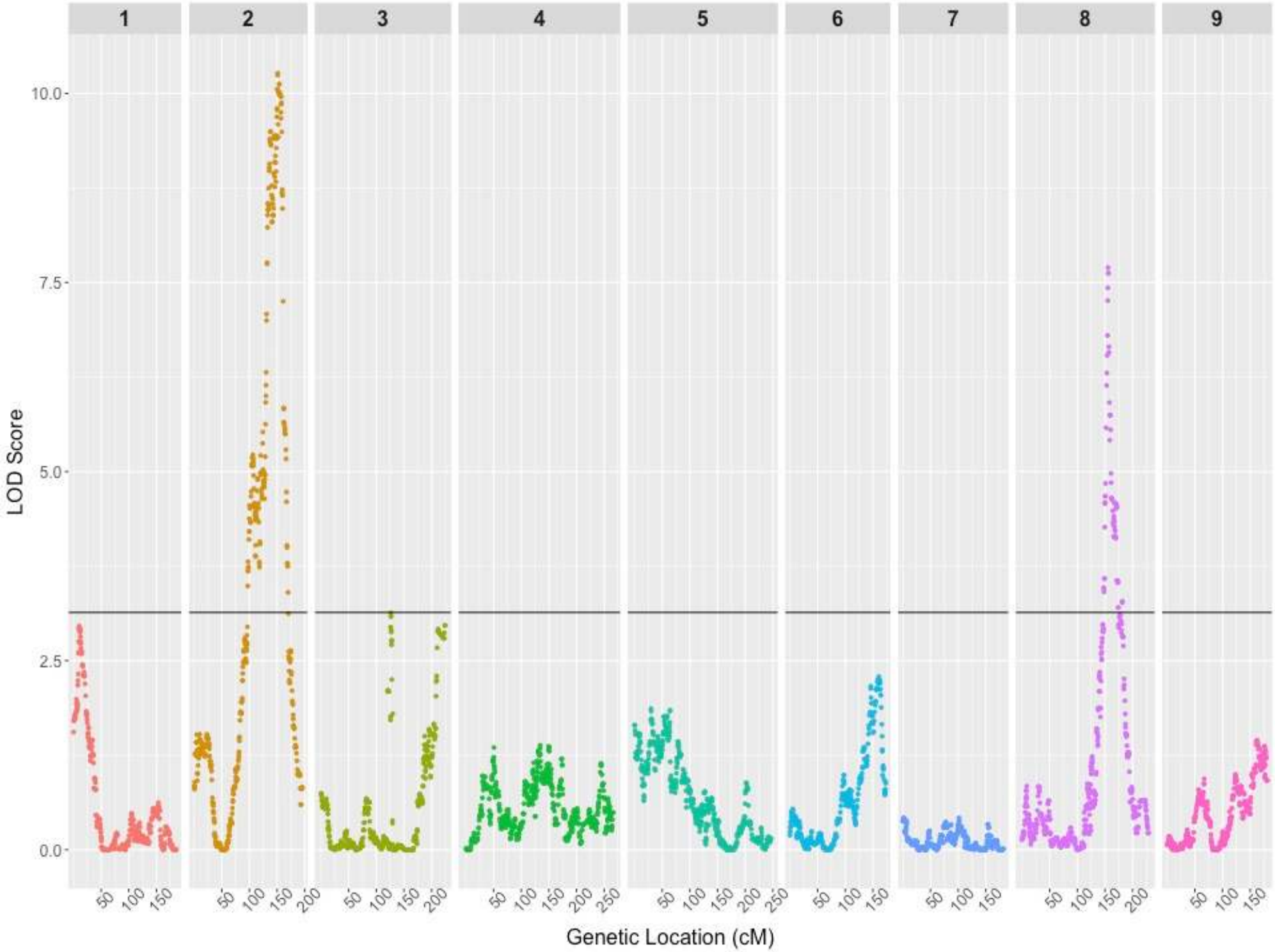

Figure 10. LOD scores of markers for peak floral opening time shown along the nine chromosomal linkage groups. The LOD threshold for significance ($p < 0.05$) calculated by 10,000 permutations is shown as a black line.

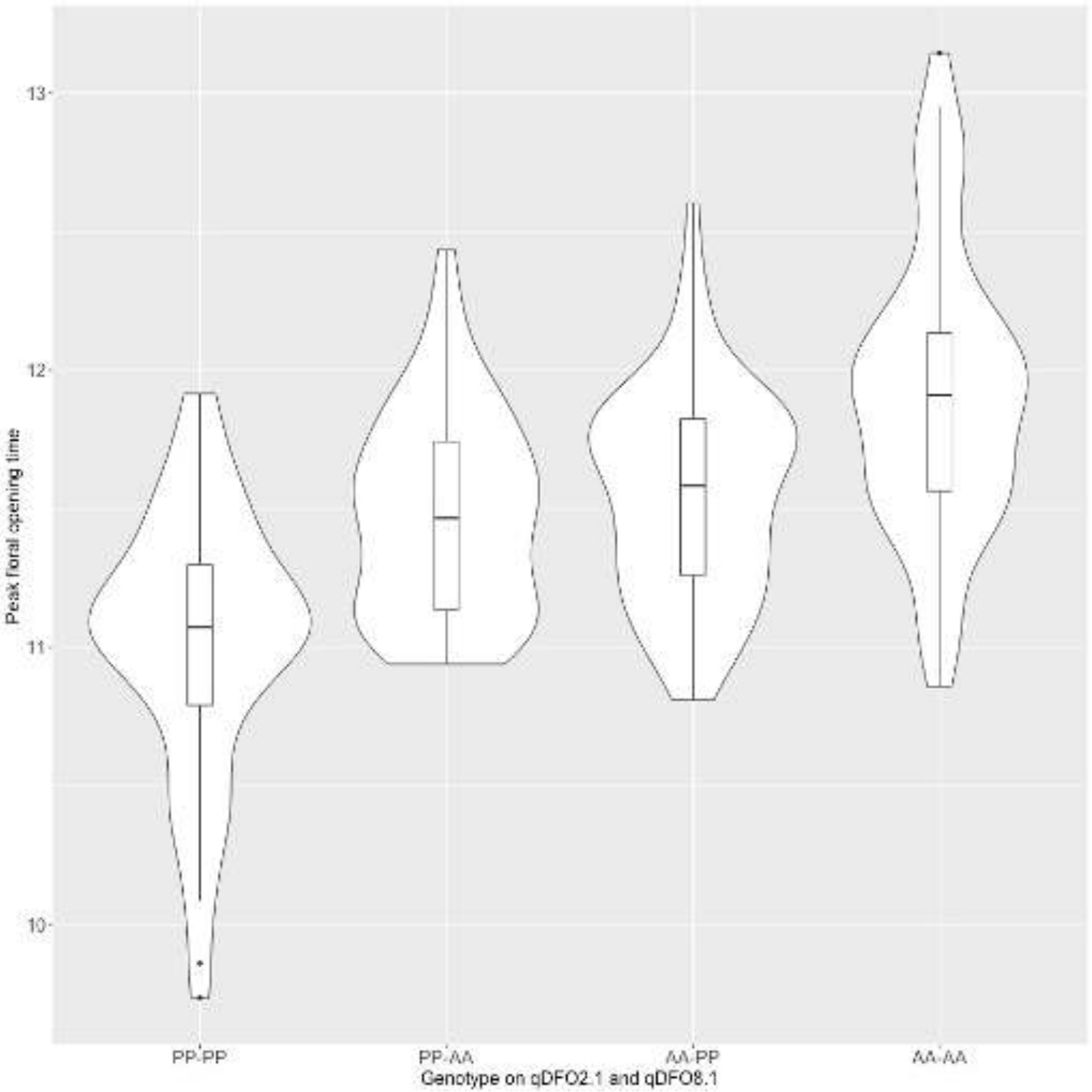

Figure 11. The additive effect of Armenian999 alleles at each QTL on peak floral opening time. The box plots represent the median and quartiles of the phenotypic distribution of each allelic combination. Widths of the violin plots represent density of samples at each phenotypic value.

Parsed Citations

Broman KW, Wu H, Sen Ś, Churchill GA (2003) R/qtl: QTL mapping in experimental crosses. Bioinformatics 19: 889–890
Pubmed: Author and Title
Google Scholar: Author Only Title Only Author and Title

Colquhoun TA, Schwieterman ML, Wedde AE, Schimmel BCJ, Marciniak DM, Verdonk JC, Kim JY, Oh Y, Gális I, Baldwin IT, et al (2011) EOBII Controls Flower Opening by Functioning as a General Transcriptomic Switch. Plant Physiol 156: 974 LP – 984
Pubmed: Author and Title
Google Scholar: Author Only Title Only Author and Title

Corbet SA, Fussell M, Ake R, Fraser A, Gunson C, Savage A, Smith K (1993) Temperature and the pollinating activity of social bees. Ecol Entomol 18: 17–30
Pubmed: Author and Title
Google Scholar: Author Only Title Only Author and Title

Covarrubias-Pazaran G (2016) Genome-Assisted Prediction of Quantitative Traits Using the R Package sommer. PLoS One 11: e0156744
Pubmed: Author and Title
Google Scholar: Author Only Title Only Author and Title

Cui X, Lu F, Li Y, Xue Y, Kang Y, Zhang S, Qiu Q, Cui X, Zheng S, Liu B, et al (2013) Ubiquitin-Specific Proteases UBP12 and UBP13 Act in Circadian Clock and Photoperiodic Flowering Regulation in Arabidopsis. Plant Physiol 162: 897 LP – 906
Pubmed: Author and Title
Google Scholar: Author Only Title Only Author and Title

van Doorn WG, Kamdee C (2014) Flower opening and closure: an update. J Exp Bot 65: 5749–5757
Pubmed: Author and Title
Google Scholar: Author Only Title Only Author and Title

van Doorn WG, van Meeteren U (2003) Flower opening and closure: a review. J Exp Bot 54: 1801–1812
Pubmed: Author and Title
Google Scholar: Author Only Title Only Author and Title

Emms DM, Kelly S (2015) OrthoFinder: solving fundamental biases in whole genome comparisons dramatically improves orthogroup inference accuracy. Genome Biol 16: 157
Pubmed: Author and Title
Google Scholar: Author Only Title Only Author and Title

Garrison E, Marth G (2012) Haplotype-based variant detection from short-read sequencing. arXiv Prepr. arXiv1207.3907
Pubmed: Author and Title
Google Scholar: Author Only Title Only Author and Title

Gugerli F (1998) Effect of elevation on sexual reproduction in alpine populations of Saxifraga oppositifolia (Saxifragaceae). Oecologia 114: 60–66
Pubmed: Author and Title
Google Scholar: Author Only Title Only Author and Title

Harada T, Torii Y, Morita S, Onodera R, Hara Y, Yokoyama R, Nishitani K, Satoh S (2010) Cloning, characterization, and expression of xyloglucan endotransglucosylase/hydrolase and expansin genes associated with petal growth and development during carnation flower opening. J Exp Bot 62: 815–823
Pubmed: Author and Title
Google Scholar: Author Only Title Only Author and Title

Herten K, Hestand MS, Vermeesch JR, Van Houdt JKJ (2015) GBSX: a toolkit for experimental design and demultiplexing genotyping by sequencing experiments. BMC Bioinformatics 16: 73
Pubmed: Author and Title
Google Scholar: Author Only Title Only Author and Title

Jégu T, Latrasse D, Delarue M, Hirt H, Domenichini S, Ariel F, Crespi M, Bergounioux C, Raynaud C, Benhamed M (2014) The BAF60 Subunit of the SWI/SNF Chromatin-Remodeling Complex Directly Controls the Formation of a Gene Loop at FLOWERING LOCUS C in Arabidopsis Plant Cell 26: 538 LP – 551

Kaihara S, Takimoto A (1980) Studies on the light controlling the time of flower-opening in Pharbitis nil. Plant Cell Physiol 21: 21–26
Pubmed: Author and Title
Google Scholar: Author Only Title Only Author and Title

Kehrberger S, Holzschuh A (2019) How does timing of flowering affect competition for pollinators, flower visitation and seed set in an early spring grassland plant? Sci Rep 9: 15593

Kuhn M (2008) Building Predictive Models in R Using the caret Package. J Stat Software; Vol 1, Issue 5 . doi: 10.18637/jss.v028.i05
Pubmed: Author and Title
Google Scholar: Author Only Title Only Author and Title

Lavelle D (2009) Genetics of Candidate Genes for Developmental and Domestication-Related Traits in Lettuce. University of California, Davis
Pubmed: Author and Title
Google Scholar: Author Only Title Only Author and Title

Li H (2013) Aligning sequence reads, clone sequences and assembly contigs with BWA-MEM. arXiv Prepr. arXiv1303.3997
Pubmed: Author and Title
Google Scholar: Author Only Title Only Author and Title

Lu Y-H, Arnaud D, Belcram H, Falentin C, Rouault P, Piel N, Lucas M-O, Just J, Renard M, Delourme R (2012) A dominant point mutation in a RINGv E3 ubiquitin ligase homoeologous gene leads to cleistogamy in Brassica napus. Plant Cell 24: 4875–4891
Pubmed: Author and Title
Google Scholar: Author Only Title Only Author and Title

Matsumoto T, Yasumoto AA, Nitta K, Yahara T, Tachida H (2013) Difference in flowering time as an isolating barrier. J Theor Biol 317: 161–167
Pubmed: Author and Title
Google Scholar: Author Only Title Only Author and Title

McElreath R (2016) Statistical rethinking : a Bayesian course with examples in R and Stan.

Nitta K, Yasumoto AA, Yahara T (2010) Variation of flower opening and closing times in F1 and F2 hybrids of daylily (Hemerocallis fulva; Hemerocallidaceae) and nightlily (H. citrina). Am J Bot 97: 261–267
Pubmed: Author and Title
Google Scholar: Author Only Title Only Author and Title

Rastas P (2017) Lep-MAP3: robust linkage mapping even for low-coverage whole genome sequencing data. Bioinformatics 33: 3726–3732
Pubmed: Author and Title
Google Scholar: Author Only Title Only Author and Title

Reid MS, Evans RY, Dodge LL, Mor Y Ethylene and silver thiosulfate influence opening of cut rose flowers. 114: 436–440

Reyes-Chin-Wo S, Wang Z, Yang X, Kozik A, Arikit S, Song C, Xia L, Froenicke L, Lavelle DO, Truco M-J, et al (2017) Genome assembly with in vitro proximity ligation data and whole-genome triplication in lettuce. Nat Commun 8: 14953
Pubmed: Author and Title
Google Scholar: Author Only Title Only Author and Title

Le Roy K, Vergauwen R, Cammaer V, Yoshida M, Kawakami A, Van Laere A, Van den Ende W (2007) Fructan 1-exohydrolase is associated with flower opening in Campanula rapunculoides. Funct Plant Biol 34: 972–983
Pubmed: Author and Title
Google Scholar: Author Only Title Only Author and Title

Sakamoto RL, Ito M, Kawakubo N (2012) Contribution of Pollinators to Seed Production as Revealed by Differential Pollinator Exclusion in Clerodendrum trichotomum (Lamiaceae). PLoS One 7: e33803
Pubmed: Author and Title
Google Scholar: Author Only Title Only Author and Title

Sandoya G V, Maisonneuve B, Truco MJ, Bull CT, Simko I, Trent M, Hayes RJ, Michelmore RW (2019) Genetic analysis of resistance to bacterial leaf spot in the heirloom lettuce cultivar Reine des Glaces. Mol Breed 39: 160
Pubmed: Author and Title
Google Scholar: Author Only Title Only Author and Title

Spindel JE, Dahlberg J, Colgan M, Hollingsworth J, Sievert J, Staggenborg SH, Hutmacher R, Jansson C, Vogel JP (2018) Association mapping by aerial drone reveals 213 genetic associations for Sorghum bicolor biomass traits under drought. BMC Genomics 19: 679
Pubmed: Author and Title
Google Scholar: Author Only Title Only Author and Title

Truco MJ, Ashrafi H, Kozik A, van Leeuwen H, Bowers J, Wo SRC, Stoffel K, Xu H, Hill T, Van Deynze A, et al (2013) An Ultra-High-Density, Transcript-Based, Genetic Map of Lettuce. G3 Genes|Genomes|Genetics 3: 617 LP – 631
Pubmed: Author and Title
Google Scholar: Author Only Title Only Author and Title

Vergauwen R, Van den Ende W, Van Laere A (2000) The role of fructan in flowering of Campanula rapunculoides. J Exp Bot 51: 1261–1266
Pubmed: Author and Title
Google Scholar: Author Only Title Only Author and Title

Wang K, Li M, Hakonarson H (2010) ANNOVAR: functional annotation of genetic variants from high-throughput sequencing data. Nucleic Acids Res 38: e164–e164
Pubmed: Author and Title
Google Scholar: Author Only Title Only Author and Title

Wang T, Pan H, Wang J, Yang W, Cheng T, Zhang Q (2014) Identification and profiling of novel and conserved microRNAs during the flower opening process in Prunus mume via deep sequencing. Mol Genet Genomics 289: 169–183

Pubmed: Author and Title
Google Scholar: Author Only Title Only Author and Title

Wimmer V, Albrecht T, Auinger H-J, Schön C-C (2012) synbreed: a framework for the analysis of genomic prediction data using R. Bioinformatics 28: 2086–2087

Pubmed: Author and Title
Google Scholar: Author Only Title Only Author and Title

Xu R, Li C, Paterson AH (2019) Multispectral imaging and unmanned aerial systems for cotton plant phenotyping. PLoS One 14: e0205083

Pubmed: Author and Title
Google Scholar: Author Only Title Only Author and Title

Zhou L, Dong L, Jia P-Y, Wang W-R, Wang L-Y (2010) Expression of ethylene receptor and transcription factor genes, and ethylene response during flower opening in tree peony (Paeonia suffruticosa). Plant Growth Regul 62: 171–179

Pubmed: Author and Title
Google Scholar: Author Only Title Only Author and Title